npj | clean water

Article

Published in partnership with King Fahd University of Petroleum & Minerals

https://doi.org/10.1038/s41545-025-00449-3

Microwave-enhanced catalytic degradation of organic compounds with silica-coated iron oxide nanocrystals via fenton-like reaction pathway

Junseok Lee[1,2,6], Seunghyun Weon[3,6], Seung Soo Steve Lee[2], Eun-tae Yun[2], Myoung Won Chung[3], Changwoo Kim[4], Hailiang Wang[5] ✉ & John D. Fortner[2] ✉

Microwave (MW)-enhanced catalytic oxidation processes are emerging and effective techniques for the degradation of organic compounds in water and wastewater treatment processes. In this study, through applied MW irradiation, monodisperse, superparamagnetic iron oxide nanocrystals (IONCs) with thin, amorphous silica coatings are demonstrated to rapidly catalyze the degradation of organic compounds in water through a thermally enhanced, Fenton−type process. For this, we precisely synthesize amorphous silica-coated various metal oxide (single domain) nanocrystals, and then evaluate the degradation of methyl orange (MO) and benzoic acid (BA), chosen as model organic molecules. We examine (and optimize) the effects of core (nanocrystal) composition, size, and concentration, along with solution pH and hydrogen peroxide (H_2O_2) concentration. Further, we describe the catalytic degradation of BA with IONCs under MW irradiation through radical scavenger controls and electron paramagnetic resonance (EPR) analysis, which support the proposed reaction mechanism. For materials evaluated, the amorphous silica coating not only prevents the loss of nanocrystal integrity but also provides a reactive, yet stable, interface between nanocrystals and bulk solutions, where the degradation of organic compounds can occur. Synthesized IONCs show high performance, which is repeatable for over five cycles without any deterioration of the nanocrystals core or metal leaching. Taken together, this research highlights the potential of enhanced MW-enhanced oxidation processes appropriately coated (i.e., designed) MW absorbers (here as superparamagnetic IONCs) for advanced water treatment.

Advanced oxidation processes (AOPs) have been widely developed and utilized for the rapid and efficient oxidation and degradation of various organic pollutants in water and wastewater treatment processes. AOPs produce highly reactive free radicals, including hydroxyl radicals, superoxide anion radicals, and sulfate radicals, which can rapidly degrade recalcitrant organic contaminants[1–3]. The most widely used AOP processes in water treatment include photocatalytic oxidation, Fenton- and Fenton−like oxidation, ozonation, and catalytic oxidation, among others[4]. In addition, new AOP technologies are emerging, such as electrochemical−based reactions, electron beam, plasma, ultrasound, and/or microwave based processes[5]. These technologies aim to maintain the advantages of traditional AOP processes while lowering chemical and energy usage (depending on water quality and pre−treatment processes)[6].

Energy input through microwave (MW) irradiation has unique advantages, including rapid heating, reduced reaction time(s), increased product selectivity, higher pollutant degradation efficiency, sustainability, and ease of control[7–9]. Based on these enhancements, MW−enhanced processes have high potential to contribute to the development of more

[1]Department of Environmental Engineering, Incheon National University, Incheon, Republic of Korea. [2]Department of Chemical and Environmental Engineering, Yale University, New Haven, CT, USA. [3]School of Health and Environmental Science, Korea University, Seoul, Republic of Korea. [4]Department of Environment and Energy Engineering, Gwangju Institute of Science and Technology, Gwangju, Republic of Korea. [5]Department of Chemistry, Yale University, New Haven, CT, USA. [6]These authors contributed equally: Junseok Lee, Seunghyun Weon. ✉e-mail: hailiang.wang@yale.edu; john.fortner@yale.edu

efficient and sustainable solutions for water and wastewater treatment. Under typical MW conditions, MW energy (1 − 300 GHz) is insufficient to break down the chemical bonds of organic compounds, and thus MW−absorbing materials are often used to improve degradation efficiency. Such materials include carbon−based materials and ferromagnetic metal or transition metal oxides[10,11]. Among these, magnetic nanoparticles (MNPs) such as iron oxide nanoparticles can be utilized for hyperthermic treatment processes, which can emit (localized, surface−based) heat when subjected to external electromagnetic irradiation (i.e., radio frequency). Effectively acting as energy 'antennas,' by efficiently absorbing MW irradiation, extreme, surface-localized heat gradients can be harnessed for new thermal treatment paradigms, different from those relying on oscillating magnetic fields[12,13]. When functionally optimized, including for magnetic susceptibility, such materials offer specificity and efficiency benefits, in addition to low−energy magnetic recovery, thus offering unique advantages compared to other MW absorbers. To the best of our knowledge, the feasibility of iron oxide nanocrystals (IONCs) as a catalyst in MW-assisted (thermal)catalytic degradation of organic compounds has not been optimized for water treatment applications.

Superparamagnetic iron oxide nanoparticles, widely used for their controllable size/shape, biocompatibility, and ease of recovery through magnetic separation, are available at an industrial scale, making them suitable for environmental remediation and catalysis-based applications[14–16]. Further, emerging green synthesis and related utilization pathways offer additional production and/or scaling opportunities[17]. For aqueous−based applications of magnetic nanocrystals, surface functionalization is crucial not only for the specific application (e.g., sorbing targeted species) but also for colloidal stability, biocompatibility, and chemical stability (i.e., preventing dissolution)[18–20]. While organic surfactants and/or polymers are widely used, their susceptibility to decomposition and/or degradation at elevated temperatures presents a significant technological limitation for MW−based particle applications which generate/rely on high heat gradients[21,22]. To address this, alternative coating materials, such as carbonaceous materials, and metal or metal oxide shell(s), including silica and gold, may be considered based on their chemical and mechanical stabilities, low toxicity, and temperature resistant properties[23]. Of these, semi−permeable silica coatings offer thermal and chemical stability along with biocompatibility, while not altering core properties (e.g., magnetization)[24–26].

In this study, we precisely prepared iron oxide nanocrystals (IONCs) with thin amorphous silica coatings as MW absorbers for thermally MW-enhanced catalysis, considering a Fenton−like process. High catalytic performance was observed for the degradation of model organic compounds, here as methyl orange (MO) and benzoic acid (BA), and explored as function of core material type and composition, core size, and catalyst concentration, as well as the role of water chemistry, including solution pH and hydrogen peroxide (H_2O_2) concentration. The role of generated radicals, as reactant(s), is described through radical scavenger experiments and EPR analyses, which support proposed reaction mechanism(s). Finally, reusability of optimized materials was clearly demonstrated through consecutive (cycled) reactions and chronoamperometry measurements, highlighting another system advantage.

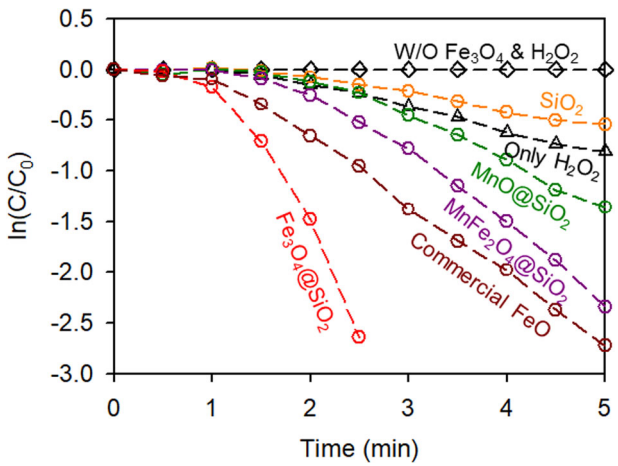

Fig. 1 | MO degradation using various types of catalysts with amorphous silica coatings under MW irradiation. Degradation of methyl orange (MO) by metal oxide nanocatalysts ($MnO@SiO_2$, $MnFe_2O_4@SiO_2$, and $Fe_3O_4@SiO_2$ NCs), bare silica nanoparticles, and commercial iron oxide with 0.75% of H_2O_2 at pH 3 under microwave (MW) irradiation. Initial concentration of MO is 10 mg/L.

Results and Discussion

Microwave−enhanced catalytic degradation of model organics

Rapid methyl orange (MO) degradation was observed with precisely engineered metal oxide nanocrystals (NCs), with thin, amorphous silica coatings, under standard microwave (MW) irradiation conditions (described above) with H_2O_2. TEM micrographs of highly monodisperse NCs, including amorphous silica-coated iron oxide, manganese oxide, and mixed manganese−iron oxide, which have the same core size (20 ± 1.2 nm), and 78 ± 6 nm bare silica nanoparticles (control), are shown in Supplementary Fig. 1. XRD data indicate that crystalline structures of 20 nm metal oxide NCs are well matched with magnetite (Fe_3O_4), manganese iron oxide ($MnFe_2O_4$, ferrite), and manganese oxide ($MnO@Mn_3O_4$), as shown in Supplementary Fig. 2. To assess catalytic performance, MO degradation was evaluated as a model organic compound, which can be simply monitored via UV−Vis spectroscopy, for a range of conditions, including the presence of hydrogen peroxide (H_2O_2, 0.75%) over time, as done in previous studies (Supplementary Fig. 3)[27]. Figure 1 illustrates the degradation of MO as a function of reaction constituents and time. In the presence of MW-absorbing particles, two distinct reaction stages are observed: an initial, relatively slow (inactive) stage (< 1 min) which is likely due to insufficient available heat, and a subsequently rapid degradation stage (> 1 min)[28,29]. For these, the rapid stage reactions follow first order kinetics (linear $\ln(C/C_0)$) as a function of reaction time (beyond the initializing point, 1 min), and core composition, with observed rate constants of 1.93 min^{-1} for $Fe_3O_4@SiO_2$ NCs, 0.654 min^{-1} for $MnFe_2O_4@SiO_2$ NCs, 0.436 min^{-1} for $MnO@SiO_2$ NCs, and 0.165 min^{-1} for SiO_2 NCs (Fig. 1, MW irradiation at 2.45 GHz, pH 3). Not only are the observed rate constants very high, but the heating/activation process via MW irradiation is also much faster than conventional bulk heating methods[30]. In addition to hyperthermic properties, IONCs are capable of initiating Fenton(−like) reaction(s) to effectively generate hydroxyl radicals for MO degradation[31]. While manganese ferrites are also considered highly effective microwave absorbers[32], lower Fenton−like reaction efficiencies have been observed with increasing Mn content (Mn containing ferrite materials compared to Fe content)[33]. Control experiments show no MO degradation without NCs and/or H_2O_2 applied; thus, MW energy applied alone is not enough to degrade MO within the time scales evaluated[34]. Further, negligible to relatively minor degradation of MO with no NCs and only H_2O_2 (0.232 min^{-1}) was observed. In contrast to commercial iron oxide nanoscale particles (50-100 nm particle size, uncoated), which undergo transformation (i.e., iron leaching) during the same reaction process, amorphous silicacoated IONCs demonstrated not only higher reaction rates but also exceptional stability (no leaching measured) for numerous cycles, which are further discussed below.

Effect of core size and concentration of IONCs on MO degradation

NC size/core was hypothesized to be a key performance variable, which was directly explored by altering the ratio of concentration of iron oleate and oleic acid (OA) during the synthesis, controlling IONC diameters from 8 to 20 nm with high monodispersity (Supplementary Fig. 4). For this, we synthesized and tested four distinct IONC sizes (8 ± 1.7, 12 ± 0.7, 16 ± 1.7, and 20 ± 2.5 nm), all coated with amorphous silica, to evaluate MO degradation at pH 3. Pseudo−first order rate constants were observed to be 1.04 min^{-1} for 8 nm, 0.418 min^{-1} for 12 nm, 0.547 min^{-1} for 16 nm, and 1.93 min^{-1} for 20 nm particles (Fig. 2a). For these reactions, we expected

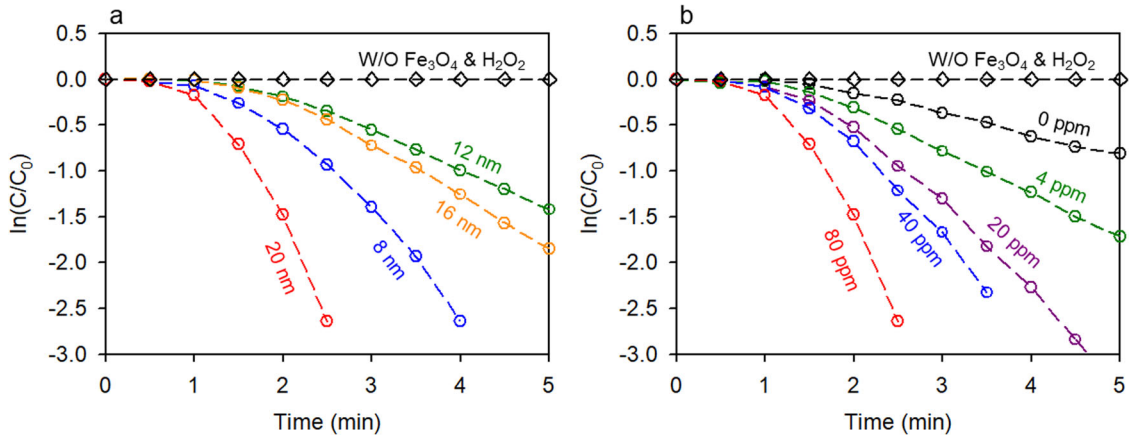

Fig. 2 | Effect of core size and concentration of iron oxide nanocrystals (IONCs) on MO degradation. a Core size and **b** concentration dependent MO degradation experiments using amorphous silica coated iron oxide nanocrystals (Fe_3O_4@SiO_2) with 0.75% of H_2O_2 at pH 3 under MW irradiation. Initial concentration of MO is 10 mg/L.

higher degradation rates with smaller core size due to their high saturation magnetization properties, which can lead to the enhanced transfer of MW to thermal energy, as shown in IONC hysteresis curves (Supplementary Fig. 5)[35]. This observation differs compared to some commercial iron oxide nanoparticles, exhibiting higher saturation magnetization with increasing of size due to the presence of organic surface coating(s), which can induce spin canting effects[36,37]. However, 20 nm IONCs exhibited the highest rate constant despite their relatively effective lower magnetism (per mass), which is likely due to the composition and corresponding oxidation state of IONCs (Fe(II)/Fe(III)). As illustrated in Supplementary Fig. 6, the ratio of Fe(II)/Fe(III) increased with increasing particle size: specifically, 1.05, 1.24, 1.02, and 2.15 for 8, 12, 16, and 20 nm sized particles, respectively. This result is consistent with previous reports by our group and others showing Fe(II) enrichment as a function of IONC size[38,39]. Higher Fe(II) concentration on the surface of IONCs can accelerate the decomposition of H_2O_2, through a Fenton(−like) reaction, resulting in comparatively higher reaction rates. We also performed IONC concentration dependent experiments (Fig. 2b) and, as expected, pseudo−first order rate constants increased with higher concentration of IONCs; 0.470 min^{-1} for 4 ppm, 0.960 min^{-1} for 20 ppm, 1.07 min^{-1} for 40 ppm, and 1.93 min^{-1} for 80 ppm, which showed a linear relationship between concentration of IONCs and rate constants (Supplementary Fig. 7a). However, excessive IONC concentration (above 80 ppm) showed negligible or even negative effects, likely due to rate limitations of redox reaction between Fe^{2+} and hydroxyl radicals generated (Supplementary Fig. 7b)[40]. This phenomenon highlights the importance of optimizing IONC concentration to achieve maximum catalytic efficiency while avoiding inefficiencies/waste associated with excess concentration(s). Based on these data, we further studied the process with 80 ppm of 20 nm amorphous silica coated IONC to better understand and optimize reaction conditions in subsequent experiments.

Effect of initial pH and H_2O_2 concentration on MO degradation

For materials described, the efficiency of MO degradation is strongly pH dependent (all other variables held constant) as rate constants decreased with increasing solution pH: 1.93, 0.256, 0.046, and 0 min^{-1} for pH 3, 4, 5, and 7, respectively (Fig. 3a). For all conditions, we confirmed that no iron was releases/dissoled from IONCs, even under low pH conditions (e.g., pH 3) as determined by ICP − MS analysis. It is well understood that Fenton reactions are highly dependent on solution pH, with higher degradation rates under acidic conditions[41,42]. The observed pH dependency also aligns with the results of Fe oxidation states (see XPS data, Supplementary Fig. 6) on the IONC surface, which are in line with typical Fenton reaction processes. The (surface) zeta potential of IONCs is also a function of solution pH, which can influence the adsorption of contaminant molecules onto the surface of the catalysts. As shown in Supplementary Fig. 8, the point of zero charge (PZC) of amorphous silica coated IONCs is approximately pH 3.4, indicating that Fe_3O_4@SiO_2 NCs are negatively charged under all experimental conditions, except at pH 3. Surface charge impacts electrostatic interactions between the catalyst surface and MO molecules, influencing their adsorption and subsequent degradation rates. Figure 3b shows the effect of H_2O_2 concentration on MO degradation under MW irradiation using silica-coated 20 nm IONCs (Fe_3O_4@SiO_2). As expected, the degradation reaction is faster with higher H_2O_2 concentrations as more hydroxyl radicals are generated, but then plateaus, due to possible diffusion−based kinetic limitations[43,44]. Corresponding reaction rate constants were 0.80, 1.93, and 1.98 min^{-1} for 0.375, 0.75, and 1.5% of H_2O_2 concentrations, respectively. We further evaluated reaction conditions at pH 3 and 0.75% of H_2O_2 in subsequent experiments, focusing on elucidating underlying reaction mechanism(s).

Reaction mechanism(s)

Experimental observations clearly indicated that IONCs with amorphous silica coatings effectively catalyze MO degradation under MW irradiation. To explore the underlying reaction mechanism(s), we also evaluated benzoic acid (BA) degradation, as an indicator of oxidizing radical production, under varied experimental conditions[45,46]. While no noticeable BA loss was observed in the presence of IONCs or H_2O_2 alone, BA was rapidly degraded in the presence of IONC, H_2O_2, and MW irradiation (IONCs/H_2O_2/MW system), similar to MO, with a first order rate constant of 1.18 min^{-1} (Fig. 4a). For this reaction, we observed stoichiometric production of 4−hydroxybenzoic acid (4−hba, Supplementary Fig. 9) as a byproduct, indicating the presence of hydroxyl radicals, as reported by others[47,48]. We hypothesize that the amorphous silica coating on the surface of iron oxide (core) not only enhances NC stability in water under MW irradiation, but also allows for the Fenton−based hydroxyl radical generation at the particle−water interface. TEM analysis showed excellent colloidal stability of silica-coated IONCs with no physical changes of IONCs before and after MW reactions (Supplementary Fig. 10), with consistent elemental mapping, suggesting no deterioration under MW irradiation (Supplementary Fig. 11). To further demonstrate interfacial interactions between IONCs and bulk solutions at/through amorphous silica coatings, we performed a strong acid treatment to IONC solution with nitric and hydrochloric acid under heating (80°C) for 2 h. Upon this treatment, we observed a resulting hollow silica structure in TEM micrographs, indicating iron dissolution and diffusion through the amorphous silica coating itself (Supplementary Fig. 12). In a related study,

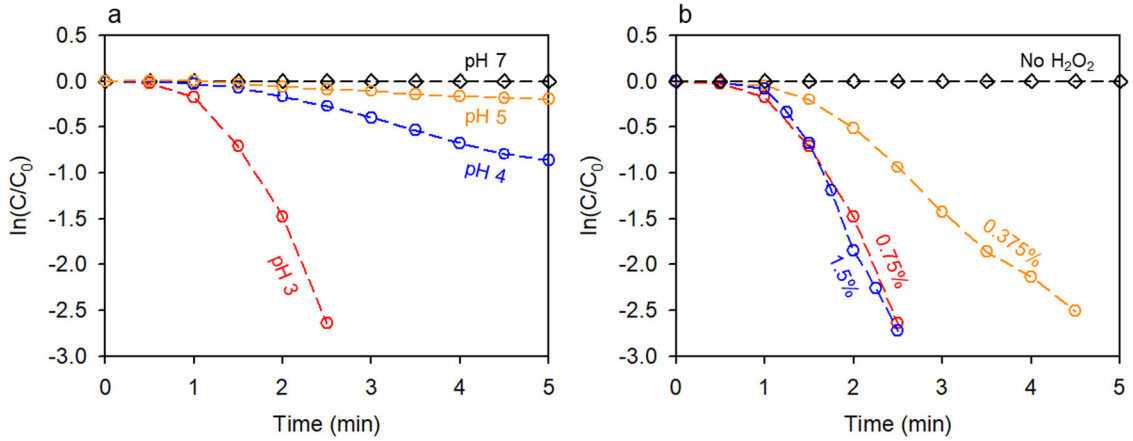

Fig. 3 | Effect of water chemistries on MO degradation. a Solution pH and **b** hydrogen peroxide (H_2O_2) concentration dependent MO degradation using amorphous silica coated iron oxide nanocrystals (Fe_3O_4@SiO_2) under MW irradiation. Initial concentration of MO is 10 mg/L.

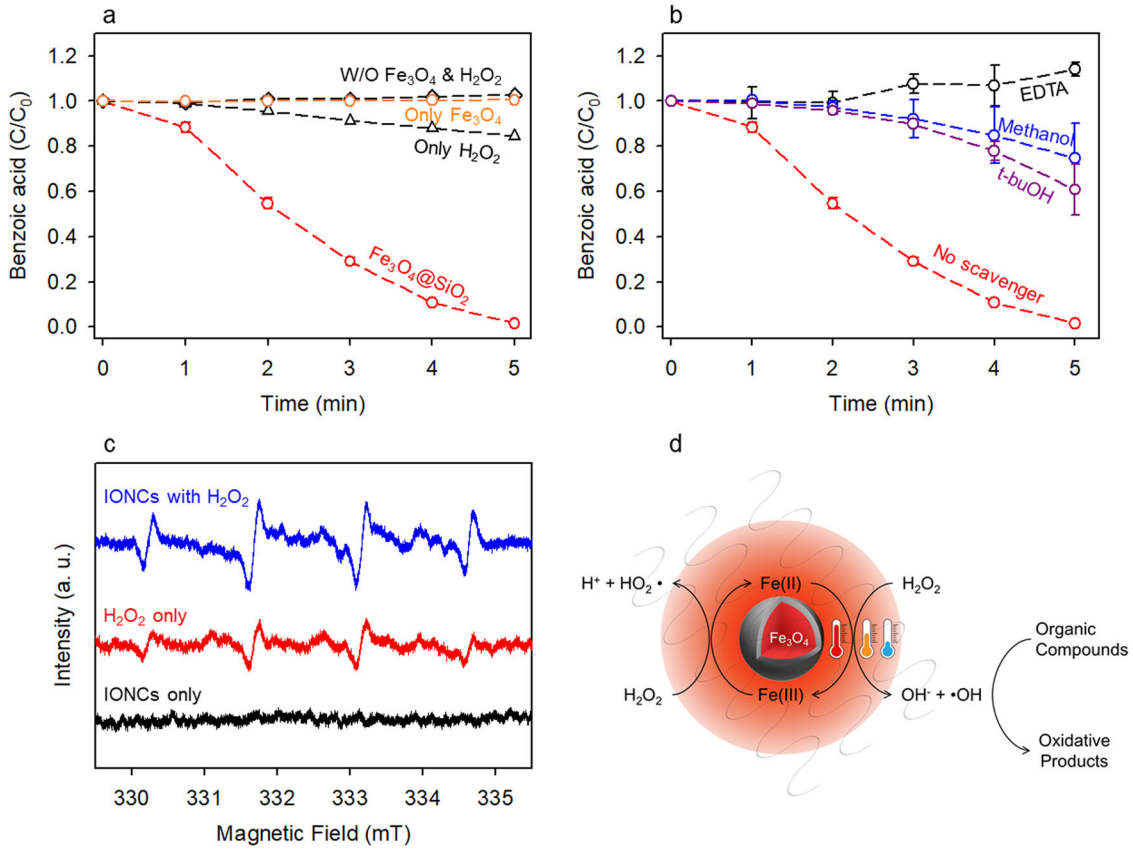

Fig. 4 | Mechanistic investigation of catalytic degradation via amorphous silica coated IONCs under MW irradiation. a Benzoic acid (BA) degradation under different experimental conditions. **b** BA degradation profiles in the presence of various scavengers including methanol, EDTA, and t−buOH, respectively. **c** Spin trap EPR analysis of three different systems; IONCs only, H_2O_2 only, and IONCs with H_2O_2, respectively, under MW irradiation ([DMPO] = 5 mM). **d** Proposed mechanisms for degradation of organic compounds using amorphous silica coated IONCs under MW irradiation.

Gan et al. presented a silica sol–gel coating technique applied to optical surfaces, enabling the adsorption of ammonia within the silica coating layer itself, which serves as a sensing mechanism for detecting ammonia in water[49]. Kim et al. demonstrated the efficacy of silica oxide coatings to provide additional space for carrying small molecules due to their pore structure, which allows for the diffusion of methylene blue into the interlayer of mesoporous silica[50]. Our findings align with these previous reports, and highlight the critical role of amorphous silica coatings in controlling the stability of IONCs while allowing for interfacial reactivity.

To further explore hydroxyl radical production, radical scavengers, including methanol, EDTA, and tert−butanol (t−buOH), were employed[51,52]. As shown in Fig. 4b, the presence of methanol, EDTA, and t−buOH inhibited the degradation of BA, with C/C$_0$ values under MW reaction (5 min) of 75%, 100%, and 61% for methanol, EDTA, and t−buOH, respectively. This result strongly suggests that hydroxyl radical plays a significant role in the reaction as observations follow a commonly observed trend for hydroxyl radical quenching effectiveness (EDTA>-methanol>t−buOH)[53]. We further confirmed hydroxyl radical generation by EPR analysis using DMPO (5 mM) as a spin−trapping agent, exploring

different system variable including IONCs alone, H_2O_2 alone, and IONC/H_2O_2 under MW irradiation. While the hydroxyl radical is clearly detected in the IONCs/H_2O_2/MW system, low or no signal was observed for IONCs or H_2O_2 when applied alone (Fig. 4c), which is also consistent with the results from degradation experiments presented in previous sections. Considering all variables explored, we propose a reaction mechanism, which is Fenton−based and synergistically enhanced by hyperthermic effect(s), for which a schematic is presented in Fig. 4d. As discussed above, hyperthermic metal oxide NCs absorbing MW radiation (via magnetic dipole rotation and spin relaxation) generate/dissipate thermal energy to the surrounding matrix[54]. This hyperthermic effect induces localized heating, thereby accelerating chemical reactions and enhancing interfacial catalytic activity. In addition to hyperthermic effects, iron oxide nanocrystals (IONCs) such as these can initiate/enable Fenton(−like) reaction(s) in the presence of H_2O_2 without thermal input[55]. We propose that ferrous iron (Fe(II)) on the surface of IONCs can be readily oxidized in the presence of H_2O_2, producing appreciable hydroxyl radical flux under MW irradiation, which results in enhanced organic degradation efficiencies. MW-IONC induced heat likely affects reactivity directly (via hot surface(s)/interfaces) and through increased mass transfer through the amorphous silica shell itself.

Recycle and reuse of MW−absorbing nanocatalysts

We evaluated (re)cycling performance of engineered, amorphous silica coated IONCs (80 ppm) for five (turnover) cycles under MW irradiation at pH 3 with 0.75% H_2O_2. Under these conditions, we observe rapid MO degradation for each of the five cycles, with reaction rates slightly decreasing (Fig. 5a). Such decline is likely due to the Fe(II) to Fe(III) ratios changing under stated reaction conditions, as it is well known that the reduction of Fe(III) to Fe(II) is much slower than the reaction of Fe(II) oxidizing Fe(III) via H_2O_2 when generating hydroxyl radicals[56,57]. We thus expect that relative Fe(II) concentrations at the IONC surface to decrease over consecutive uses, resulting in decreasing rate constants. Supporting this, we observed no pH changes and/or iron release (into the bulk solution) over the five cycles. To further understand material reuse potential, chronoamperometric measurements were conducted to explore consecutive electrochemical reaction on an anode chamber, whereby targeted materials, here as IONC@SiO_2 and commercial Fe_3O_4, were coated on the carbon paper at 0.5 V (vs Ag/AgCl)[58,59]. Upon the first injection of H_2O_2, similar current change was observed for both engineered IONC@SiO_2 and commercial Fe_3O_4 due to electron transfer and hydroxyl radical generation. Interestingly, we observed similar current change with engineered IONC@SiO_2 coated electrode upon subsequent addition of H_2O_2, while relatively lower or no obvious change occurred for the commercial Fe_3O_4 coated electrode (Fig. 5b). Such behavior supports potential novel applications that rely on surface-controlled hydroxyl radical production for numerous reaction cycles (compared to commercial Fe_3O_4). Based on these results, it is clear that amorphous silica-coated IONC enhanced, MW−based catalytic reactions offer unique process advantages for novel treatment technologies and should be further evaluated and optimized.

Methods

Materials

Iron (III) chloride hexahydrate ($FeCl_3{\cdot}6H_2O$, 97%), manganese (II) chloride tetrahydrate ($MnCl_2{\cdot}4H_2O$, 99.99%), oleic acid (OA, 90%), 1−octadecene (90%), ethanol (99.9%), acetone (99.5%), and hexane (98.5%), cyclohexane (99%), Igepal CO − 630, polyvinylpyrrolidone (PVP, MW = 360 kDa), ammonium hydroxide (NH_4OH, 28–30%), tetraethoxy orthosilicate (TEOS, 99.999%), hydrogen peroxide (H_2O_2, 30%), methyl orange (MO), benzoic acid (99.5%) were purchased from Sigma Aldrich. Sodium oleate (97%) was obtained from TCI America.

Preparation of amorphous silica coated metal oxide and ferrite nanocrystals

Nanocrystalline metal oxides (iron oxide, manganese oxide, and iron manganese oxide (ferrites)) were synthesized based on the method reported previously[60,61]. For details, metal (iron and manganese) oleate precursors were synthesized by reacting metal chloride with sodium oleate in mixture of ethanol, water, and hexane at 60 °C for 4 h. Iron oxide, manganese oxide, and iron-manganese oxide nanocrystals were then synthesized using metal oleates (as metal precursors) decomposition at 320 °C for a desired time (typically 1 h). Their size and composition(s) were tuned by various reaction conditions such as, the precursor concentrations, the ratio of the precursor to the surfactant (oleic acid), and the reaction time. Organically synthesized metal oxides were purified using ethanol, acetone, and hexane over 6 times. The synthesized nanocrystals were then, functionalized with high molecular weight amphiphilic polymer (Igepal CO−630) for further silica encapsulation; the silica coating was processed by TEOS injection to the solution containing Igepal CO−630 adsorbed metal oxides[62,63]. The phase transferred metal oxide nanocrystals were purified using ethanol and DI water and finally stored in DI water. As a control material, bare silica nanoparticles were synthesized based on the Stöber method, where TEOS was injected to the co-solvent of ethanol and DI water at pH 11 and the reaction was kept at 25 °C for 2 h under N_2 flow[64,65].

Material characterization

Size and shape of metal oxide nanocrystals (NCs) were characterized through Transmission Electron Microscope (TEM, Tecnai Osiris, FEI), where size was obtained using Image Pro Plus 6.0 software (Media

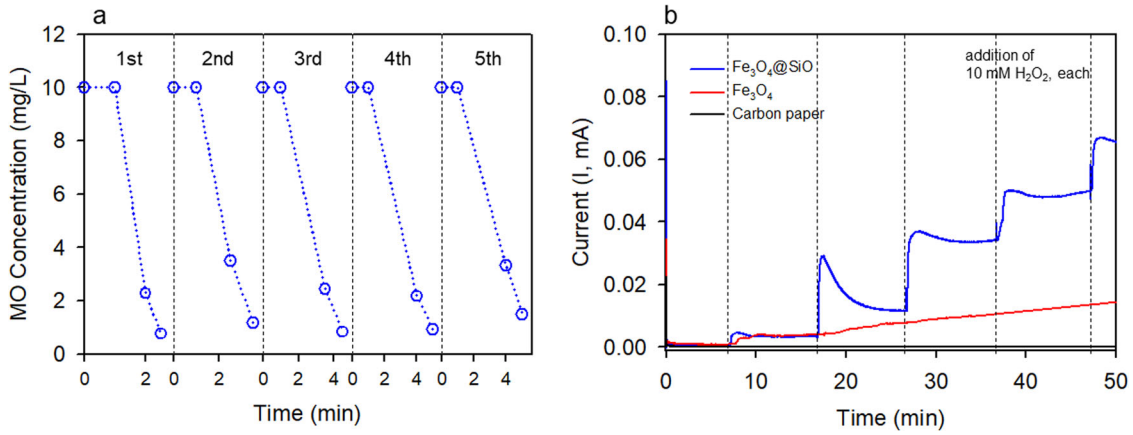

Fig. 5 | Recycle and reuse of MW−absorbing nanocatalysts. a Repetition tests of methyl orange (MO) degradation using engineered amorphous silica coated iron oxide nanocrystals (IONC@SiO_2) over 5 cycles. **b** Chronoamperometery scan at 0.5 V under the pulsed addition of 10 mM hydrogen peroxide (5 steps; *dotted line*) on anode coated with IONC@SiO_2 NCs at every 10 min.

Cybernetics) by counting over ca. one thousand particles on the image from TEM. The elemental mapping of NCs was also acquired by TEM using energy dispersive spectroscopy (EDS) analysis. X−ray diffraction (XRD) patterns of synthesized metal oxide NCs were obtained from 20° to 80° of 2θ using Bruker d8 Advance X−ray diffractometer with a Cu kα radiation (1.54 Å). Concentrations of NCs were measured by an inductively coupled plasma mass spectrometer (ICP−MS, NexION 5000, PerkinElmer) after acidification of samples with mixture of hydrochloric and nitric acids (1 N) for 2 h under heating (80–90 °C) before analyses. The hydrodynamic diameter and zeta potential of surface functionalized NCs were measured by Dynamic Light Scattering (DLS, NanoBrook Omni, Brookhaven Instruments). The oxidation state of iron (Fe) is evaluated by X−ray Photoelectron Spectroscope (XPS, PHI VersaProbe II Scanning XPS Microprobe) analysis. For EPR analysis, 5,5−dimethyl−1−pyrroline-N−oxide (DMPO) was used as a spin trapping agent for hydroxyl radical. The EPR spectra were recorded using an electron spin resonance spectrometer (ESR, JES −X310, JEOL).

Degradation tests for organic compounds under microwave irradiation

We performed degradation experiments for organic compounds, here as methyl orange (MO) and benzoic acid (BA), using amorphous silica encapsulated metal oxide NCs under microwave (MW) irradiation (2.45 GHz, 270 watts). For details, the NCs containing solution (typically 80 mg/L) in a quartz vial was placed in the microwave oven. Before MW irradiation, a target organic pollutant (10 mg/L and 1 mM as initial concentration for MO and BA) and a desired amount of H_2O_2 (from 0 to 1.5%) were injected to the NCs solution and adjusted pH to 3 ± 0.2 at room temperature (nearly 20°C). Solution pH was adjusted using HNO_3 and NaOH before the experiments. During reactions under MW irradiation, sample aliquots were extracted at predetermined time intervals, subsequently separation of NCs by centrifugation, and supernatant was collected for further analysis. Concentrations of MO and BA in supernatants were tracked/monitored by UV−Vis spectroscopy (Cary 100, Agilent Technologies) and HPLC (Agilent 1260 Infinity II, Agilent Technologies). Reusability and stability of NCs were tested by consecutive five cycles of degradation experiments. To further investigate repeatability of IONCs, electrochemical experiments were conducted by chronoamperometry method on potentiostat (VMP3, BioLogic) in a two−chamber system with a cation exchange membrane separating the cathode and anode. The corresponding anode materials were fabricated using amorphous silica coated IONCs solutions with Nafion as an adherent and a conducting binder dropwise added on carbon paper (0.37 mm, 5 wt%), in which Pt and Ag/AgCl electrodes were chosen as cathode and reference electrodes, respectively. Chronoamperometric measurements were carried out with a constant potential of 0.5 V in 0.1 M potassium hydroxide (KOH) as the electrolyte, and a desired amount of H_2O_2 (10 mM) was injected at predetermined time interval on the anode side.

Data availability

The datasets used and/or analysed during the current study available from the corresponding author on reasonable request.

Received: 10 December 2024; Accepted: 27 February 2025;
Published online: 03 April 2025

References

1. Ma, D. et al. Critical review of advanced oxidation processes in organic wastewater treatment. *Chemosphere* **275**, 130104 (2021).
2. Wang, J. & Wang, S. Reactive species in advanced oxidation processes: formation, identification and reaction mechanism. *Chem. Eng. J.* **401**, 126158 (2020).
3. Lee, J., von Gunten, U. & Kim, J.-H. Persulfate-based advanced oxidation: critical assessment of opportunities and roadblocks. *Environ. Sci. Technol.* **54**, 3064–3081 (2020).
4. Rekhate, C. V. & Srivastava, J. Recent advances in ozone-based advanced oxidation processes for treatment of wastewater-A review. *Chem. Eng. J. Adv.* **3**, 100031 (2020).
5. Stefan, M. I. Advanced oxidation processes for water treatment: fundamentals and applications. (IWA publishing, 2017).
6. Hodges, B. C., Cates, E. L. & Kim, J.-H. Challenges and prospects of advanced oxidation water treatment processes using catalytic nanomaterials. *Nat. Nanotechnol.* **13**, 642–650 (2018).
7. Remya, N. & Lin, J.-G. Current status of microwave application in wastewater treatment—A review. *Chem. Eng. J.* **166**, 797–813 (2011).
8. Cao, M. et al. Recent advances in microwave-enhanced advanced oxidation processes (MAOPs) for environmental remediation: A review. *Chem. Eng. J.* **471**, 144208 (2023).
9. Xia, H. et al. A review of microwave-assisted advanced oxidation processes for wastewater treatment. *Chemosphere* **287**, 131981 (2022).
10. Liu, S. et al. Anchoring Fe3O4 Nanoparticles on Carbon Nanotubes for Microwave-Induced Catalytic Degradation of Antibiotics. *ACS Appl. Mater. Interfaces* **10**, 29467–29475 (2018).
11. Yin, C., Cai, J., Gao, L., Yin, J. & Zhou, J. Highly efficient degradation of 4-nitrophenol over the catalyst of Mn2O3/AC by microwave catalytic oxidation degradation method. *J. Hazard. Mater.* **305**, 15–20 (2016).
12. Laurent, S., Dutz, S., Häfeli, U. O. & Mahmoudi, M. Magnetic fluid hyperthermia: focus on superparamagnetic iron oxide nanoparticles. *Adv. colloid interface Sci.* **166**, 8–23 (2011).
13. Greff, J. & Babadagli, T. Use of nano-metal particles as catalyst under electromagnetic heating for in-situ heavy oil recovery. *J. Pet. Sci. Eng.* **112**, 258–265 (2013).
14. Gonzalez-Moragas, L., Yu, S.-M., Murillo-Cremaes, N., Laromaine, A. & Roig, A. Scale-up synthesis of iron oxide nanoparticles by microwave-assisted thermal decomposition. *Chem. Eng. J.* **281**, 87–95 (2015).
15. Besenhard, M. O. et al. Continuous production of iron oxide nanoparticles via fast and economical high temperature synthesis. *React. Chem. Eng.* **5**, 1474–1483 (2020).
16. Li, W., Wu, J., Lee, S. S. & Fortner, J. D. Surface tunable magnetic nano-sorbents for carbon dioxide sorption and separation. *Chem. Eng. J.* **313**, 1160–1167 (2017).
17. Singh, J. et al. Green'synthesis of metals and their oxide nanoparticles: applications for environmental remediation. *J. nanobiotechnology* **16**, 1–24 (2018).
18. Levard, C., Hotze, E. M., Lowry, G. V. & Brown, G. E. Jr Environmental transformations of silver nanoparticles: impact on stability and toxicity. *Environ. Sci. Technol.* **46**, 6900–6914 (2012).
19. Li, Y., Zhang, W., Niu, J. & Chen, Y. Surface-Coating-Dependent Dissolution, Aggregation, and Reactive Oxygen Species (ROS) Generation of Silver Nanoparticles under Different Irradiation Conditions. *Environ. Sci. Technol.* **47**, 10293–10301 (2013).
20. Lee, J. et al. Delineating the role of surface grafting density of organic coatings on the colloidal stability, transport, and sorbent behavior of engineered nanoparticles. *Environ. Sci.: Nano* **11**, 578–587 (2024).
21. Hwang, C. et al. Facile organic surfactant removal of various dimensionality nanomaterials using low-temperature photochemical treatment. *RSC Adv.* **9**, 730–737 (2019).
22. López-Pérez, L. et al. Process Intensification of Mesoporous Material's Synthesis by Microwave-Assisted Surfactant Removal. *ACS Sustain. Chem. Eng.* **8**, 16814–16822 (2020).
23. Lu, A.-H. et al. Precise synthesis of discrete and dispersible carbon-protected magnetic nanoparticles for efficient magnetic resonance imaging and photothermal therapy. *Nano Res.* **9**, 1460–1469 (2016).
24. Guerrero-Martínez, A., Pérez-Juste, J. & Liz-Marzán, L. M. Recent progress on silica coating of nanoparticles and related nanomaterials. *Adv. Mater.* **22**, 1182–1195 (2010).
25. Morel, A.-L. et al. Sonochemical Approach to the Synthesis of Fe3O4@SiO2 Core−Shell Nanoparticles with Tunable Properties. *ACS Nano* **2**, 847–856 (2008).

26. Zhuravlev, L. The surface chemistry of amorphous silica. Zhuravlev model. *Colloids Surf. A: Physicochemical Eng. Asp.* **173**, 1–38 (2000).
27. Kim, C., An, S., Lee, J., Zeng, Q. & Fortner, J. D. Engineering Graphene Oxide Laminate Membranes for Enhanced Flux and Boron Treatment with Polyethylenimine (PEI) Polymers. *ACS Appl. Mater. Interfaces* **11**, 924–929 (2019).
28. Shiying, Y. et al. A novel advanced oxidation process to degrade organic pollutants in wastewater: Microwave-activated persulfate oxidation. *J. Environ. Sci.* **21**, 1175–1180 (2009).
29. Bhandari, P. S. & Gogate, P. R. Microwave assisted persulfate induced degradation of sodium dodecyl benzene sulfonate. *Korean J. Chem. Eng.* **36**, 2000–2007 (2019).
30. Langa, F., de la Cruz, P., de la Hoz, A., Díaz-Ortiz, A. & Díez-Barra, E. Microwave irradiation: more than just a method for accelerating reactions. *Contemp. Org. Synth.* **4**, 373–386 (1997).
31. Chen, F., Xie, S., Huang, X. & Qiu, X. Ionothermal synthesis of Fe3O4 magnetic nanoparticles as efficient heterogeneous Fenton-like catalysts for degradation of organic pollutants with H2O2. *J. Hazard. Mater.* **322**, 152–162 (2017).
32. Hakeem, A. et al. Manganese-based spinel ferrites for microwave absorption. *J. Mater. Sci.: Mater. Electron.* **32**, 2557–2563 (2021).
33. Hussain, S., Aneggi, E. & Goi, D. Catalytic activity of metals in heterogeneous Fenton-like oxidation of wastewater contaminants: a review. *Environ. Chem. Lett.* **19**, 2405–2424 (2021).
34. Xu, D., Cheng, F., Lu, Q. & Dai, P. Microwave enhanced catalytic degradation of methyl orange in aqueous solution over CuO/CeO_2 catalyst in the absence and presence of H_2O_2. *Ind. Eng. Chem. Res.* **53**, 2625–2632 (2014).
35. Bakoglidis, K., Simeonidis, K., Sakellari, D., Stefanou, G. & Angelakeris, M. Size-dependent mechanisms in AC magnetic hyperthermia response of iron-oxide nanoparticles. *IEEE Trans. Magn.* **48**, 1320–1323 (2012).
36. Baaziz, W. et al. Magnetic iron oxide nanoparticles: reproducible tuning of the size and nanosized-dependent composition, defects, and spin canting. *J. Phys. Chem. C.* **118**, 3795–3810 (2014).
37. Darbandi, M. et al. Nanoscale size effect on surface spin canting in iron oxide nanoparticles synthesized by the microemulsion method. *J. Phys. D: Appl. Phys.* **45**, 195001 (2012).
38. Kim, C., Lee, S. S., Ghosh, A., Lee, J. & Fortner, J. D. Cetyltrimethylammonium bromide – Oleic acid (CTAB-OA) bilayer coated iron oxide nanocrystals for enhanced chromium (VI) photoreduction via ligand-to-metal charge transfer mechanism. *Chem. Eng. J.* **431**, 133938 (2022).
39. Park, J. et al. Ultra-large-scale syntheses of monodisperse nanocrystals. *Nat. Mater.* **3**, 891–895 (2004).
40. Annabi, C. et al. Degradation of enoxacin antibiotic by the electro-Fenton process: optimization, biodegradability improvement and degradation mechanism. *J. Environ. Manag.* **165**, 96–105 (2016).
41. Jung, Y. S., Lim, W. T., Park, J. Y. & Kim, Y. H. Effect of pH on Fenton and Fenton-like oxidation. *Environ. Technol.* **30**, 183–190 (2009).
42. Vasquez-Medrano, R., Prato-Garcia, D. & Vedrenne, M. in *Advanced Oxidation Processes for Waste Water Treatment* (eds Suresh C. Ameta & Rakshit Ameta) 89–113 (Academic Press, 2018).
43. Babuponnusami, A. & Muthukumar, K. Removal of phenol by heterogenous photo electro Fenton-like process using nano-zero valent iron. *Sep. Purif. Technol.* **98**, 130–135 (2012).
44. Wang, H. et al. Rapid decomplexation of Ni-EDTA by microwave-assisted Fenton reaction. *Chem. Eng. J.* **381**, 122703 (2020).
45. Chen, Y., Miller, C. J., Xie, J. & Waite, T. D. Challenges relating to the quantification of ferryl (IV) ion and hydroxyl radical generation rates using methyl phenyl sulfoxide (PMSO), phthalhydrazide, and benzoic acid as probe compounds in the homogeneous fenton reaction. *Environ. Sci. Technol.* **57**, 18617–18625 (2023).
46. Rayaroth, M. P., Lee, C.-S., Aravind, U. K., Aravindakumar, C. T. & Chang, Y.-S. Oxidative degradation of benzoic acid using Fe0-and sulfidized Fe0-activated persulfate: a comparative study. *Chem. Eng. J.* **315**, 426–436 (2017).
47. Feng, Y. et al. Degradation of contaminants by Cu+-activated molecular oxygen in aqueous solutions: evidence for cupryl species (Cu3+). *J. Hazard. Mater.* **331**, 81–87 (2017).
48. Zrinyi, N. & Pham, A. L.-T. Oxidation of benzoic acid by heat-activated persulfate: effect of temperature on transformation pathway and product distribution. *Water Res.* **120**, 43–51 (2017).
49. Gan, W. et al. Rapid and sensitive detection of ammonia in water by a long period fiber grating sensor coated with sol-gel silica. *Opt. Express* **30**, 33817–33825 (2022).
50. Kim, B. S., Chen, Y.-T., Srinoi, P., Marquez, M. D. & Lee, T. R. Hydrogel-encapsulated mesoporous silica-coated gold nanoshells for smart drug delivery. *Int. J. Mol. Sci.* **20**, 3422 (2019).
51. Zhang, J. et al. Unveiling the collective effects of moisture and oxygen on the photocatalytic degradation of m-Xylene using a titanium dioxide supported platinum catalyst. *Chem. Eng. J.* **439**, 135747 (2022).
52. Duan, L. et al. Efficient photocatalytic PFOA degradation over boron nitride. *Environ. Sci. Technol. Lett.* **7**, 613–619 (2020).
53. Gupta, A. D., Bansal, V. K., Babu, V. & Maithil, N. Chemistry, antioxidant and antimicrobial potential of nutmeg (Myristica fragrans Houtt). *J. Genet. Eng. Biotechnol.* **11**, 25–31 (2013).
54. Mishra, R. R. & Sharma, A. K. Microwave–material interaction phenomena: heating mechanisms, challenges and opportunities in material processing. *Compos. Part A: Appl. Sci. Manuf.* **81**, 78–97 (2016).
55. Du, L., Wang, X. & Wu, J. Degradation of tri(2-chloroethyl)phosphate by a microwave enhanced heterogeneous Fenton process using iron oxide containing waste. *RSC Adv.* **8**, 18139–18145 (2018).
56. Pignatello, J. J., Oliveros, E. & MacKay, A. Advanced oxidation processes for organic contaminant destruction based on the Fenton reaction and related chemistry. *Crit. Rev. Environ. Sci. Technol.* **36**, 1–84 (2006).
57. Zhou, P. et al. Fast and long-lasting iron (III) reduction by boron toward green and accelerated fenton chemistry. *Angew. Chem. Int. Ed.* **59**, 16517–16526 (2020).
58. Yun, E.-T., Yoo, H.-Y., Bae, H., Kim, H.-I. & Lee, J. Exploring the role of persulfate in the activation process: radical precursor versus electron acceptor. *Environ. Sci. Technol.* **51**, 10090–10099 (2017).
59. Yun, E.-T. et al. Oxidation of organic pollutants by peroxymonosulfate activated with low-temperature-modified nanodiamonds: Understanding the reaction kinetics and mechanism. *Appl. Catal. B: Environ.* **237**, 432–441 (2018).
60. Lee, S. S. et al. Surface functionalized manganese ferrite nanocrystals for enhanced uranium sorption and separation in water. *J. Mater. Chem. A* **3**, 21930–21939 (2015).
61. Kim, C. et al. Surface functionalized nanoscale metal oxides for arsenic(v), chromium(vi), and uranium(vi) sorption: considering single- and multi-sorbate dynamics. *Environ. Sci.: Nano* **7**, 3805–3813 (2020).
62. Selvan, S. T., Tan, T. T. & Ying, J. Y. Robust, non-cytotoxic, silica-coated CdSe quantum dots with efficient photoluminescence. *Adv. Mater.* **17**, 1620–1625 (2005).
63. Selvan, S. T., Patra, P. K., Ang, C. Y. & Ying, J. Y. Synthesis of silica-coated semiconductor and magnetic quantum dots and their use in the imaging of live cells. *Angew. Chem.* **119**, 2500–2504 (2007).
64. Stöber, W., Fink, A. & Bohn, E. Controlled growth of monodisperse silica spheres in the micron size range. *J. colloid interface Sci.* **26**, 62–69 (1968).
65. Ghimire, P. P. & Jaroniec, M. Renaissance of Stöber method for synthesis of colloidal particles: new developments and opportunities. *J. Colloid Interface Sci.* **584**, 838–865 (2021).

Acknowledgements

This work was supported by NIEHS grant # P42ES023716 and # P42ES033815. ICP-MS, IC and TOC analyzer were provided by the Yale

Analytical and Stable Isotope Center (YASIC), XPS and XRD analysis was provided by Yale West Campus Materials Characterization Core (MCC), and TEM was provided by Yale Institute for Nanoscience and Quantum Engineering (YINQ) at Yale University. This work was also supported by the National Research Foundation of Korea(NRF) grant funded by the Korea government(MSIT) (RS-2024-00406500).

Author contributions

J.L.: Conceptualization, Methodology, Experiments, Writing, S.W.: Methodology, E.P.R. analysis, Writing, S.sS.L.: Conceptualization, Synthesis, Writing, E.-t.Y.: Electrochemical experiments, M.W.C.: E.P.R. analysis, C.K.: Data analysis, Hailiang Wang: Reviewing, Editing, J.D.F.: Supervision, Resources, Writing, Reviewing, Editing.

Competing interests

The authors declare no competing interests.

Additional information

Supplementary information The online version contains supplementary material available at https://doi.org/10.1038/s41545-025-00449-3.

Correspondence and requests for materials should be addressed to Hailiang Wang or John D. Fortner.